

NINETEENTH EUROPEAN ROTORCRAFT FORUM

Paper n°N2

**CRASH ANALYSIS AND CORRELATION WITH TEST OF A
COMPOSITE HELICOPTER SUB-FLOOR STRUCTURE**

by

**V. GIAVOTTO, G. SALA, M. ANGHILERI
AEROSPACE ENGINEERING DEPARTMENT
POLITECNICO DI MILANO
ITALY**

**September 14-16, 1993
CERNOBBIO (COMO)
ITALY**

**ASSOCIAZIONE INDUSTRIE AEROSPAZIALI
ASSOCIAZIONE ITALIANA DI AERONAUTICA E ASTRONAUTICA**

CRASH ANALYSIS AND CORRELATION WITH TEST OF A COMPOSITE HELICOPTER SUB-FLOOR STRUCTURE

by

V. GIAVOTTO, G. SALA, M. ANGHILERI
AEROSPACE ENGINEERING DEPARTMENT
POLITECNICO DI MILANO
ITALY

Abstract

The paper reports a comprehensive activity carried out at Aerospace Engineering Department of Politecnico di Milano within the frame of a cooperation with Agusta Helicopters. The basic aim of the project was to develop and validate procedures, as well as to acquire experience on the design of advanced energy absorption structures. The final object of the study is the design and testing of an optimised composite helicopter sub-floor structure. The first stage of the research program consisted in the testing of simple cylindrical impact coupons and structure sub-components for a first choice of the most promising materials and design concepts. The second phase consisted in an accurate material characterisation, through dynamic tests performed at different strain rates on simple specimens, to obtain reliable material models suited for a subsequent finite element crash analysis. With these material models, numerical analysis was performed on the crash of both the sub-components tested during the experimental phase and the relatively large sub-floor assemblies. The results of the tests and the numerical simulations show a fairly good agreement, both in terms of load - deflection characteristic and of failure and energy absorption mechanisms.

Introduction

Helicopters were among the first flight machines to adopt composite materials and so doing very serious structural problems found a solution, such as fatigue in rotor blades. For helicopter fuselage, weight saving is, if possible, even more important than for fixed wing aircrafts; several attempts have been made to design and produce helicopter structures entirely made of composite materials (ACAP) with the aim to reduce weight and improve structural efficiency. Furthermore, helicopters, owing to their typical operating envelope, were the first flying machines which had to comply to crashworthiness requirements [1]. Thus, the problem to be faced consists in evaluating the convenience to adopt the composites in the main crashworthy demanding helicopter structures (e.g. subfloors), that is to assess if no weight increase takes place or, better, if some weight saving is possible. Due to the novelty of the problem no *conventional* or well assessed solutions are yet available, neither for material and structural philosophies, nor for crashworthiness design tools. For these reasons a wide study has been performed, aimed at first to characterise candidate composite material systems (reinforcement, matrix, stacking sequence and degree of hybridisation) using the simplest meaningful coupons (tubular); then to assess and compare different design solutions for both components and assemblies; and finally to evaluate the numerical tools to be used for crash simulations and design, taking into account the lack of reliably composite materials laws able to reproduce the dynamic and failure behaviour.

Preliminary experimental tests on tubes

The experimental activity has been at first performed on 200 tubular specimens, 200 mm high, 80 and 160 mm in diameter, having D/t ratios varying between 24 and 175, the dimensions and wall thicknesses being comparable to typical sizes of helicopter structures components [2-5]. Tubular coupons have been adopted due to their intrinsic axi-symmetry which allows an easy analysis of energy absorbing mechanisms; besides the results can be compared to the ones obtained by other authors; finally, the production of composite tubes is relatively easy and cheap, by means of wrapping and or filament winding techniques [6-8]. The specimens have been wrapped with different types of epoxy prepreg, namely: carbon unidirectional and fabric, aramidic unidirectional and fabric and hybrid carbon-aramidic, each characterised by different orientation, stacking sequence and foam core presence. Core volume of foamed specimens have been 50% reduced to avoid anomalous laminate failure due to the foam incompressibility reached during dynamic test. The upper edge of cylinders have been triggered by means of a 60° bevel, to induce a more regular failure mechanism and to decrease the initial load peak [9-11]. A drop weight test machine has been used; accelerations and displacements have been measured by means of an accelerometer and an encoder at a sampling rate of 10 KHz; the accelerometer signal has been low-pass filtered at 1 KHz. Three tests have been performed for each type of specimens and for each load condition, namely: quasi static, 6, 8, 10 m/s impact velocity, at a constant energy of 3.5 KJ. The failure of Carbon specimens is due to interlaminar and intralaminar cracks along hoop strips characterised by local buckling; the instability starts at the bevelled edge and its length of diffusion depends on D/t ratio; final failure is due to cyclic instabilities followed by interlaminar delaminations and intralaminar cracks. If compared to aluminium alloys coupon, carbon tubes show a more uniform trend of sustained load and, for comparable D/t values, an higher average dynamic strength; the tests have also shown the brittleness of graphite specimens, which do not maintain a satisfactory post-crash structural integrity. Considering $[\pm 45^\circ]_s$ (unidirectional) cylinders, the tests have shown a specific energy absorption (SEA) decrease when increasing D/t value (Fig 1); besides, SEA impact velocities (V_i) curves show that absorbed energy increases when increasing V_i , while their slope increases for high values of D/t (Fig 2); finally load uniformity ratio (LUR) notably reduces (Fig 3) for high V_i . For $[\pm 45^\circ]_s$ (fabric) cylinders, SEA diminishes when increasing D/t values (Fig 4); the energy absorbed during quasi-static test is remarkably higher than the energy absorbed during dynamic tests and it does not depend on impact velocities: in fact energy absorbing capability does not notably vary with V_i (Fig 5), while LUR lessens when V_i increase (Fig 6). Tests on multi-axial fabric-unidirectional hybrid carbon specimens have been performed as well; in particular coupons having 50% angle-ply and 50% on-axis layers have shown an higher energy absorbing capability than simple $\pm 45^\circ$ tubes; furthermore, fabric unidirectional hybrid specimens behave better than fabric ones, being their energy absorption capabilities comparable to unidirectional specimen, but possessing in the meantime a much more appreciable post-impact integrity. Aramidic tubes show a behaviour very similar to the aluminium alloys one: in fact the crushing is due to a cyclic development of local instabilities, which gives rise to the typical 'accordion-like' or diamond shape; moreover aramidic coupons are characterised by a good post crash integrity. Test results have shown that SEA decreases when D/t increases (Fig 7); V_i does not notably influence both SEA (Fig 8) and LUR (Fig 9). Hybrid specimens, made with both aramidic and graphite layers have been tested as well; the substitution of graphite outer plies with aramidic layers always improves coupons crashworthiness; in particular hybrid coupons possess SEA and LUR values quite comparable to graphite ones, but meanwhile have a much higher post-crash integrity. Finally, the behaviour of hybrid coupons has been studied varying D/t values and impact velocity: the result show that SEA does not notably depend on both D/t and V_i , while LUR remarkably decreases when V_i increases. The tests performed on *foamed cylinders* show that the increase in crushing strength due to the core stabilising effect does not counterbalance the weight increase. In comparison with the same coupons tested without foam, a general decrease of crashworthiness parameters is observed. In conclusion the tests have shown that failure mechanism strongly depends on the kind, size and shape of the trigger, which is able to induce a more regular crushing load time-history. D/t ratio values are strongly correlated with both SEA and LUR: D/t

increasing, absorbed energy decreases, while LUR increases. Specimens made of carbon unidirectional absorb more and more energy when impact velocity increases, being $[\pm 45^\circ/0^\circ]_s$ (unidirectional) the more efficient stacking sequence. Graphite coupons show a brittle behaviour and their failure produce fragments and splinters; their ability to absorb energy during a dynamic test is not remarkably affected by impact energy and in any case it has resulted lower than energy absorbed during quasi-static tests; carbon fabric specimens are less efficient than the coupons made of unidirectional tape. Aramidic fabric cylinders show a behaviour very close to aluminium alloys tubes: they both are characterised by load fluctuations during crushing phenomenon, good post-crash integrity, plastic deformations and low dependence on impact velocity; besides, in general, aramidic cylinders are not so efficient as graphite ones in energy absorption. The coupons made of on-axis unidirectional graphite tapes and angle-ply aramidic and graphite fabrics layers have shown the best crashworthiness performances; in fact their SEA and LUR values do not notably depend on impact velocity, thanks to aramidic and graphite fabrics, while SEA values are quite comparable to unidirectional graphite ones; besides outer aramidic fabric confers an appreciable post-impact integrity. Finally, all composite specimens have shown different failure modes in quasi-static and dynamic tests: for this reason the crashworthiness of a composite structure cannot be correctly evaluated by means of quasi static-tests.

Preliminary experimental tests on beams

Preliminary experimental tests have been performed on short (320 mm) and long (960) beams, characterised by the same structural shape of helicopter real subfloor frames and spars [12-14]. Four kinds of beams have been tested, namely:

- Type A: hybrid graphite-aramide/epoxy beams having $[45^\circ_{kf}/45^\circ_{gf}/0^\circ_{gu}]$ sinusoidal web and $[45^\circ_{kf}/0^\circ_{gu}/45^\circ_{gf}/45^\circ_{kf}]$ flanges;
- Type B: beams having $[45^\circ_{kf}/45^\circ_{gf}]_s$ flat hybrid web stabilised with $[45^\circ_{kf}/90^\circ_{gu}]$ foamed circular cylinders and $[45^\circ_{kf}/0^\circ_{gu}/45^\circ_{gf}/45^\circ_{kf}]$ hybrid flanges;
- Type C: the same as type B, but $[45^\circ_{kf}]$ flat web does not interrupt at foamed cylinders, each of them containing four $[45^\circ_{gf}/90^\circ_{gu}]_s$ angular stiffeners; the flanges stacking sequence is $[45^\circ_{kf}/0^\circ_{gu}/45^\circ_{kf}]$;
- Type D: hybrid beams, made of two superimposed C-shaped elements, giving rise to an upper $[45^\circ_{gf}/0^\circ_{gu}/45^\circ_{gf}/0^\circ_{gu}/45^\circ_{gf}]$, a central $[45^\circ_{kf}/45^\circ_{gf}/0^\circ_{gf}/45^\circ_{gf}/0^\circ_{gu}/45^\circ_{gf}/0^\circ_{gu}/45^\circ_{gf}]$ and a lower $[45^\circ_{kf}]$ flange.

Static crushing tests on short beams

Type A (Fig 10): the failure of specimens starts with the buckling of web free edges, followed by overall buckling of central weave; possibly longer beams should not suffer so much of free-edge-effects, leading to higher sustained load; a good post-crash integrity has been observed; type B (Fig 11): the beams fails due to the contemporaneous and sudden failure of the stabilising cylinders; during crushing mechanism, outer aramidic layers have continuously folded, leading to a satisfactory post-crash integrity; type C (Fig 12): the final failure of these beams has been preceded by three intermediate failures at lower load levels, then failure has been completed by free-edges crushing and cylinders walls cleavage; a good post-crash integrity has been observed type D (Fig 13): the behaviour of these beams has been characterised by premature buckling of the lower web at a very low load level, followed by a constant elastic deflection, completely recovered once the load has been removed. In general, beams having flat web and stabilising cylinders have shown to be the most efficient, reaching the highest SEA values (10 kJ/kg), 30% higher than sinusoidal web beams. As far as LUR values are concerned, type B specimens have shown the best behaviour (3.019), while type A beams possess the highest SE (stroke efficiency) performances (85% available height crushed during load application).

Static bending tests on long beams

To evaluate bending behaviour of the beams, two coupons have been tested in four points bending for each structural shape.

Type A beams fail because of elastic buckling of the upper flange, which also induces a notable overall warping of the beam; these effects are completely recovered once the load is removed; peak load values have shown to be very dispersed. Failures of type B beams, although at very scattered load values, are both due to buckling of upper flange occurring between two contiguous cylinders, followed by compressive failure of the flange itself close to the mean cross-section; apart from this very localised damage, the beams remain intact. The failure of beams belonging to type C is due to upper flange buckling as well, but in this case flange breaks near to load application points; flange failure is then followed by web elastic instability; a satisfactory repetitivity of peak load values has been shown. To obtain a stiffness parameter suitable to compare bending behaviour of the beams, IFS (Initial Flexural Stiffness) has been computed from load vs. deflection curves; type A beams show a satisfactory repetitivity, while values relevant to type B and C are very scattered.

Dynamic crushing tests on short beams

For beams of type A, at 8 m/s impact velocity, failure has been due to overall instability of the sinusoidal web; consequently, the crushing of the coupons has not been homogeneous, remaining large parts of the web intact. In the case of 10 m/s impact velocity, coupons have shown performances quite similar, but with lower initial peak and smoother crushing mechanism (Fig 14). Crash tests on type B specimens at 8 m/s has led to total crushing of both foam core and flat web between stabilising cylinders. Foam reaches incompressibility threshold and causes the failure of cylindrical walls, which do not contribute in energy absorption. Tests at 10 m/s give results quite similar, but less dispersed; besides, crashworthiness performances show a slight improvement if compared to the ones obtained at lower impact velocity (Fig 15). Failure of type C beams during dynamic test at both 8 and 10 m/s impact velocity starts at stabilising cylinders and is due to eulerian buckling of inner stiffeners, which in turn deform and damage the outer cylindrical walls; an appreciable LUR value and post-impact integrity have been shown (Fig 16). In conclusion, beams belonging to type B have shown the best dynamic behaviour, as far as SEA, LUR and SE values. However, it should be desirable to avoid hoop failures of cylinders, which produce parts of material not contributing to energy absorption mechanisms. Beams of type C, having graphite inner stiffeners and aramidic web have shown a satisfactory crashworthiness behaviour as well, and the use of pure aramidic web has conferred a better post-crash integrity, as well as a smoother crushing phenomenon. This typology deserves to be further investigated, in order to assess the possible contribution of a trigger, devoted to reduce the load peak due to eulerian buckling of graphite inner stiffeners. Type A beams have shown the highest SE values, due to complete separation of large parts of the web, which lead to notable coupons shortening, besides they possess a satisfactory SAE and LUR behaviour; for these reasons this kind of beams, modified with a suitable trigger device, has been chosen to perform numerical simulations and to prepare complete subfloor structure.

Experimental material characterisation

Tensile static tests

Static tests have been performed on $[0^\circ]$ graphite tape graphite and $[0^\circ/90^\circ]$ Kevlar fabric, $[\pm 45^\circ]$ coupons to evaluate mechanical behaviour of the materials up to load ultimates. Seven different lay-up have been tested using the standard specimen made of eight plies with glass-epoxy tabs bonded with 3M AF-163-2K adhesive. Load and deformations have been measured by means of strain gauges and extensometers. Experiments have been performed in two steps: firstly only load ultimates have been measured, then tests have been worked out using strain gauges and load cells and stress-strain curves (σ - ϵ , τ - γ) have been recorded. Extensometers have been used to measure $[0^\circ]$ and $[90^\circ]$ longitudinal characteristics, while Poisson ratio and G moduli have been measured by means of strain gauges. The results of tensile tests are shown in tab 1.

Compressive static tests

Once again two series of experiments have been performed: firstly main elastic characteristics have been measured : E_{long} , G and ν ; then only load ultimates load have been evaluated: in this case a coupon of different shape has been chosen in order to avoid eulerian instability. The same instrumentation as for tensile tests has been used. The results of compressive tests are reported in tab 1.

Dynamic Tests

High speed tensile tests have been performed to evaluate composite strain rate sensitivity. It is well known that isotropic homogeneous materials, like steel or aluminium alloys, show a sensibility to the strain rate (bibliography); this behaviour can be well modelled by finite element codes available for crash simulation (Copwer-Simonds law), while composites are always modelled as elastic-brittle and no strain-rate-dependent materials. Several tests have been performed on composites dog-bone coupons to evaluate strain dependence. Strain rates ranging from 2 to 300 s^{-1} have been investigated. During the tests, loads and displacements have been recorded, by means of load cells, laser interferometers and LVDTs. The results are reported in (Figs 17-20). A dependence of strength ultimates on strain rates have been shown, but further investigation performed on a larger statistical base and on different coupons shape, is deserved to assess high strain rate behaviour of composite material.

Material constitutive and damage model

Static tests have been simulated to calibrate FEM (PAM-CRASH) composite model. Only static tests have been simulated because composite constitutive law implemented in the code does not allow to reproduce any strain rate sensitivity. Composites have been modelled with unidirectional tape, while fabrics have been represented by means of two superimposed unidirectional layers. The material stiffness and strength has been obtained by two phases spatial superimposition: an orthotropic 'matrix' phase and a monodimensional 'fibre' phase, each possessing its own constitutive and damage law: respectively orthotropic elastic-brittle or brittle with micro-cracks for 'matrix' and monodimensional elastic-brittle for 'fibre'. The stresses are calculated distinctly in each phase and the damage can propagate separately in each phase. The damage law modifies the elastic modulus according to the relation:

$$E(\varepsilon) = E_0 (1 - d(\varepsilon))$$

where: E_0 is the initial elastic modulus

$d(\varepsilon)$ is the damage function, expressed as:

$$d(\varepsilon) = d_v(\varepsilon_v) + d_s(\varepsilon_s)$$

where ε_v is the volumetric and ε_s is the deviatoric deformation;

for the fibres only volumetric damage exists and $\varepsilon_s = \varepsilon^f$.

The damage law is obtained imposing that d is zero up to an initial value, than it rises linearly up to the value d_l and than up to d_u (fig). A first problem to be faced consists in choosing the right stiffness parameters for unidirectional tapes in order to obtain the desired fabric mechanical characteristics. These parameters have been evaluated by means of CLT (classical lamination theory) in order to give the overall behaviour obtained in $[0^\circ]$ and $[\pm 45^\circ]$ experimental tests, solving the inverse problem from laminate characteristics to lamina E, G and ν values. Then fibres and matrix characteristics have been calculated using mixture rule. The numerical values used in the expressions of constitutive laws are reported in tabs 2-7.

Numerical simulations of material characterisation

These preliminary simulations have been performed modelling the specimens used in experimental tests by means of 250 shell elements having the material characteristics reported above. The coupons have been constrained at one edge, while a 200 mm/s on axis constant speed has been imposed to the nodes belonging to the other edge. Internal loads at the two edges and deformations of elements in the middle of the specimen have been recorded during the simulations. Numerical and experimental results are summarised in tabs 8,9.

Numerical simulations of sine wave beam dynamic tests

This work has intended to study the behaviour of sine wave beam by means of FEM simulations [15-17], using the material constitutive laws assessed above, as well as to compare the numerical results to the experimental ones [18-20]; sine wave beam model is shown in (Fig 21), while lamination and materials used are reported in (Fig 22). The beam has been modelled using 1312 shell elements; each fabric layer has been described by means of two superimposed unidirectional layers; in total 4 composite materials have been utilised. The beam has been placed between two *rigid walls*, one stationary with infinite mass and the other possessing a 111 Kg mass and a 8.1 m/s velocity, reproducing experimental conditions; all the nodes belonging to the model have been defined as slave nodes for the two rigid walls and a 0.2 friction coefficient between nodes and rigid walls has been adopted. Rigid wall normal force time history, the velocity time history and the load vs displacement curve, along with the experimental one are reported in (Fig 23). All signals have been acquired at a 20 Khz sampling rate and filtered with a 5 Khz low-pass filter. A good agreement between experimental and simulated first load peak has been shown, but after this point, the simulation is unable to fit the experimental curve, owing to the fact that, after first peak web graphite unidirectional damage parameter reaches maximum allowable value: consequently the web cannot sustain any more load and the structure collapses. The same simulation has been performed on a sine wave beam presenting a trigger in the graphite unidirectional web. The same results have been obtained, being the first load peak well simulated and, after damage, the web prevented from sustaining any load. To correct this behaviour, due to load perfect axiality, shape imperfections, introduced by means of series of variable amplitude sine functions, have been superimposed to the original geometry. So doing the value of damage after first peak has been lowered, but the structure does not behave in a completely correct way.

Conclusion

Finally some conclusions can be drawn; the experimental analysis performed on simple tubular specimens has shown that the most efficient energy absorbing laminate (in terms of SEA, LUR, SE and post impact integrity as well) as a hybrid stacking sequence, made of inner unidirectional carbon tapes and outer angle-ply aramidic fabrics, in order to fully exploit the capabilities of both highly energy absorbing graphite fibres and tough and resilient Kevlar reinforcement. The dynamic tests on short beams have demonstrated that the best compromise in energy absorbing performances are reached by sine wave type, which joints quite satisfactory LUR capability and appreciable SEA and SE behaviour. Besides this kind of beams is simpler to produce and assemble than the other kinds of specimens and does not show the problems due to foam incompressibility; finally, very efficient trigger devices can be easily incorporated into its design. Preliminary evaluation of crash numerical simulation tools has pointed out the important role played by dynamic behaviour of the materials, in terms of the influence exerted by high strain rates which activate the viscoelastic behaviour, especially as far as polymeric matrices are concerned. Numerical simulations performed up to now on sine wave coupons has succeeded in successfully reproduce first peak load, but not yet satisfactorily the

remaining part of load deflection curve; the work is now on-progress in order to better fit the experimental results, especially concerning shear type damage and consequent energy absorbing mechanisms. Moreover six-full scale subfloors of different designs are now ready to be experimentally tested and the corresponding FEM model (54,000 shells elements and 300,000 d.o.f) (Fig 24) will to be evaluated as soon as damage constitutive law, set up by means of simple test-beds, will be completely assessed.

References

1. MIL-STD-1290 , Light fixed and rotary wing aircraft crashworthiness.-1974
2. J.D. Cronkhite. Design of airframe structures for crash impact.
3. G.L.Farley , Energy absorption of composite materials, Journal of Composite Material, Vol 17.1983
4. G.L. Farley , Effect of fibre and matrix maximum strain on the energy absorption of composite materials, Journal of Composite Material, Vol 10.1986
5. G.L. Farley , Effect of specimen geometry on the energy absorption capability of composite material 1986.
6. C.M.Kinderwater , Energy absorbing qualities of fibre reinforced plastic tubes, National Specialists Meeting composite structures of the American Helicopter Society 1983.
7. J.K. Sen , Designing for a crashworthy all-composite helicopter fuselage, Journal of the American Helicopter Society, Vol 32 1987.
8. C.M.Kinderwater , Quasi -static and dynamic crushing of energy absorbing materials and structural component with the aim of improving helicopter crashworthiness, Seventh European Rotorcraft and powered lift aircraft Forum 1981.
9. V.Giavotto, C.Caprile, G. Sala, The design of helicopter crashworthiness, 66th Meeting of SMP AGARD, Luxemburg, May 1-6 1988.
10. P.H. Thornton , Energy absorption in composite structures, Journal of Composite Materials, Vol. 13 1979.
11. P.H. Thornton, P.J. Edwards , Energy absorption in composite tubes. Journal of Composite Materials, Vol. 16 1982.
12. J.K. Sen, C.C. Dremann, Design Development Tests for Composite Crashworthy Helicopter Fuselage, 30th National SAMPE symposium 3/85
13. C.M. Kinderwater, Crash Impact Behaviour and Energy Absorbing Capability of Composite Structural Components, 30th National SAMPE Symposium 3-85
14. C.M. Kinderwater, H. Georgi, U. Korber, Crashworthy Design of Aircraft Subfloor Structural Components, AGARD paper Preprint 66th AGARD Structures and Materials Panel, Luxemburg may 1-6 1988
15. C.H. Harper , Evolving Crashworthiness Design Criteria, 66th Meeting of the SMP AGARD , Luxemburg, may 1-6 1988
16. M.M. Sadeghi, Crashworthiness Design Methods Applicable at Concepts Stage, 66th meeting of the SMP AGARD, Luxemburg, may 1-6 1988
17. F. Och, Crashworthiness Activity on MMB Helicopters, 66th Meeting of the SMP AGARD, Luxemburg may 1-6 1988
18. J.Frese, D. Nitschke, Crushing Behaviour of Helicopter Subfloor Structure, 66th Meeting of SMP AGARD, Luxemburg may 1-6 1988
19. C.M Kinderwater, A. Getl, R. Muller, Crash investigations with subcomponents of a helicopter lower airframe sections, 66th Meeting SMP AGARD , Luxeburg may 1-6 1988
20. G.Sala, M. Anghileri, Analytical and Experimental Evaluation of finite element models for crash analysis, in SUSI II, P.S. Bulson editor, Computational Mechanics publications Thomas Telford 1992

| | Tension | | | Compression | | |
|-----------------------------|---------------|-----------------|---------------|---------------|-----------------|---------------|
| | Graphite tape | Graphite fabric | Kevlar fabric | Graphite tape | Graphite fabric | Kevlar fabric |
| E11 [kg/mm ²] | 13354 | 6403 | 3057 | 11376 | 5510 | 2896 |
| E22 [kg/mm ²] | 785 | 6403 | 3057 | 785 | 5510 | 2896 |
| E33 [kg/mm ²] | 785 | 785 | 785 | 785 | 785 | 785 |
| G12 [kg/mm ²] | 438 | 449 | 248 | 438 | 482 | 248 |
| v21 | 0.31 | 0.028 | 0.071 | 0.309 | 0.03 | 0.051 |
| σu [kg/mm ²] | 116.9 | 57.2 | 47.3 | 88.3 | 55.3 | 18.3 |
| E45° [kg/mm ²] | | 1411 | 726 | | 1214 | 688 |
| σu45° [kg/mm ²] | | 22.4 | 18.9 | | 21.8 | 18.5 |

tab 1 : Results of tensile and compressive tests

| | Tension | Compression |
|--|----------|-------------|
| E11 ^m [kg/mm ²] | 158.0 | 152.6 |
| E22 ^m [kg/mm ²] | 783.7 | 783.7 |
| E33 ^m [kg/mm ²] | 783.7 | 783.7 |
| G12 ^m [kg/mm ²] | 438.0 | 438.0 |
| G13 ^m [kg/mm ²] | 438.0 | 438.0 |
| G23 ^m [kg/mm ²] | 438.0 | 438.0 |
| v12 | 0.018223 | 0.021323 |
| v13 | 0.018223 | 0.021323 |
| v23 | 0.018223 | 0.021323 |

tab 2 : matrix elastic characteristic (graphite unidirectional for graphite tapes)

| | Tension | Compression |
|------------------------------|----------|-------------|
| ε _{x1} ^m | .9 | .9 |
| ε _{x2} ^m | .9 | .9 |
| ε _{x3} ^m | .9 | .9 |
| d _{x1} ^m | 0.0 | 0.0 |
| d _{x2} ^m | 0.0 | 0.0 |
| ε _{y1} ^m | 0.007242 | 0.0045 |
| ε _{y2} ^m | 0.007242 | 0.0045 |
| ε _{y3} ^m | 0.007242 | 0.0045 |
| d _{y1} ^m | 0.5 | 0.5 |
| d _{y2} ^m | 1.0 | 1.0 |
| ε _{x1} ^f | 0.012498 | 0.007762 |
| ε _{x2} ^f | 0.012498 | 0.007762 |
| ε _{x3} ^f | 0.012498 | 0.007762 |
| d _{x1} ^f | 0.5 | 1.0 |
| d _{x2} ^f | 0.5 | 1.0 |

tab 3 : graphite tapes matrix and fibres damage law

| | Tension | Compression |
|--|---------|-------------|
| E11 ^m [kg/mm ²] | 158.0 | 152.6 |
| E22 ^m [kg/mm ²] | 711.3 | 783.7 |
| E33 ^m [kg/mm ²] | 711.3 | 783.7 |
| G12 ^m [kg/mm ²] | 394.9 | 438.0 |
| G13 ^m [kg/mm ²] | 394.9 | 438.0 |
| G23 ^m [kg/mm ²] | 394.9 | 438.0 |
| v12 | 0.01482 | 0.016032 |
| v13 | 0.01482 | 0.016032 |
| v23 | 0.01482 | 0.016032 |

tab 4 : matrix elastic characteristics (graphite unidirectional for graphite fabric)

| | Tension | Compression |
|------------------------------|----------|-------------|
| ε _{x1} ^m | .9 | .9 |
| ε _{x2} ^m | .9 | .9 |
| ε _{x3} ^m | .9 | .9 |
| d _{x1} ^m | 0.0 | 0.0 |
| d _{x2} ^m | 0.0 | 0.0 |
| ε _{y1} ^m | 0.013888 | 0.032105 |
| ε _{y2} ^m | 0.064706 | 0.032105 |
| ε _{y3} ^m | 0.064706 | 0.032105 |
| d _{y1} ^m | 0.5873 | 0.5 |
| d _{y2} ^m | 1.0 | 1.0 |
| ε _{x1} ^f | 0.008926 | 0.010009 |
| ε _{x2} ^f | 0.008926 | 0.010009 |
| ε _{x3} ^f | 0.008926 | 0.010009 |
| d _{x1} ^f | 0.5 | 1.0 |
| d _{x2} ^f | 0.5 | 1.0 |

tab 5 : graphite fabric matrix and fibre damage law

| | Tension | Compression |
|----------------------------------|----------|-------------|
| E_{11}^m [kg/mm ²] | 145.4 | 116.8 |
| E_{22}^m [kg/mm ²] | 761.6 | 759.8 |
| E_{33}^m [kg/mm ²] | 761.6 | 759.8 |
| G_{12}^m [kg/mm ²] | 203.7 | 193.0 |
| G_{13}^m [kg/mm ²] | 203.7 | 193.0 |
| G_{23}^m [kg/mm ²] | 203.7 | 193.0 |
| ν_{12} | 0.040562 | 0.040903 |
| ν_{13} | 0.040562 | 0.040903 |
| ν_{23} | 0.040562 | 0.040903 |

tab 6: matrix elastic characteristics (kevlar unidirectional for kevlar fabric)

| | Tension | Compression |
|-------------------|----------|-------------|
| ϵ_{y1}^m | 9 | 9 |
| ϵ_{y2}^m | 9 | 9 |
| ϵ_{y3}^m | 9 | 9 |
| d_{y1}^m | 0.0 | 0.0 |
| d_{y2}^m | 0.0 | 0.0 |
| ϵ_{x1}^m | 0.030817 | 0.047955 |
| ϵ_{x2}^m | 0.060000 | 0.047955 |
| ϵ_{x3}^m | 0.060000 | 0.047955 |
| d_{x1}^m | 0.3166 | 0.5 |
| d_{x2}^m | 1.0 | 1.0 |
| ϵ_{y1}^f | 0.015395 | 0.006287 |
| ϵ_{y2}^f | 0.015395 | 0.006287 |
| ϵ_{y3}^f | 0.015395 | 0.006287 |
| d_{y1}^f | 0.5 | 0.5 |
| d_{y2}^f | 1.0 | 1.0 |

tab 7 : kevlar fabric matrix and fibre damage law

| | Tension | | Compression | |
|----------------|------------------|------------------|------------------|------------------|
| | Exper. | Numer. | Exper. | Numer. |
| Orient. 0° | E=6403 | E=6393 | E=5510 | E=5546 |
| | $\sigma_u=57.2$ | $\sigma_u=57.03$ | $\sigma_u=55.30$ | $\sigma_u=54.94$ |
| Orient. 45° | E=1411 | E=1414 | E=1214 | E=1368 |
| | $\sigma_u=22.41$ | $\sigma_u=22.67$ | $\sigma_u=21.80$ | $\sigma_u=24.86$ |

tab 8 :Graphite fabric: Numerical and experimental elastic moduli and ultimate stress

| | Tension | | Compression | |
|----------------|------------------|------------------|------------------|------------------|
| | Exper. | Numer. | Exper. | Numer. |
| Orient. 0° | E=3057 | E=3053 | E=2896 | E=2916 |
| | $\sigma_u=47.3$ | $\sigma_u=47.07$ | $\sigma_u=18.30$ | $\sigma_u=18.13$ |
| Orient. 45° | E=726 | E=722 | E=688 | E=709 |
| | $\sigma_u=18.91$ | $\sigma_u=18.49$ | $\sigma_u=18.50$ | $\sigma_u=20.64$ |

tab 9: Kevlar fabric: Numerical and experimental elastic moduli and ultimate stress

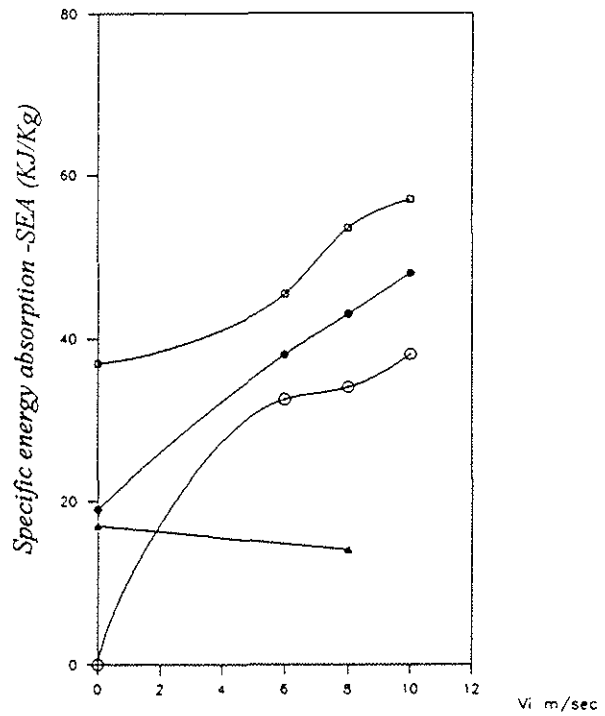
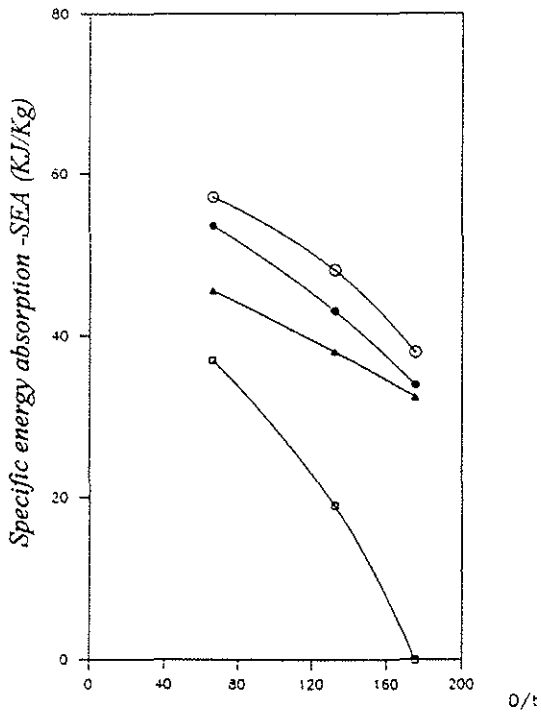


Fig 1: SEA dependence with D/t (graphite unidirectional) Fig 2: SEA dependence with Vi (graphite unidirectional)

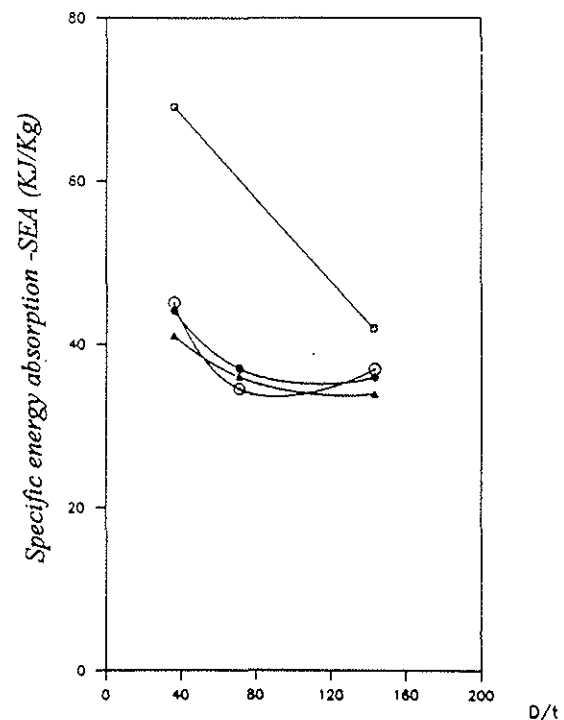
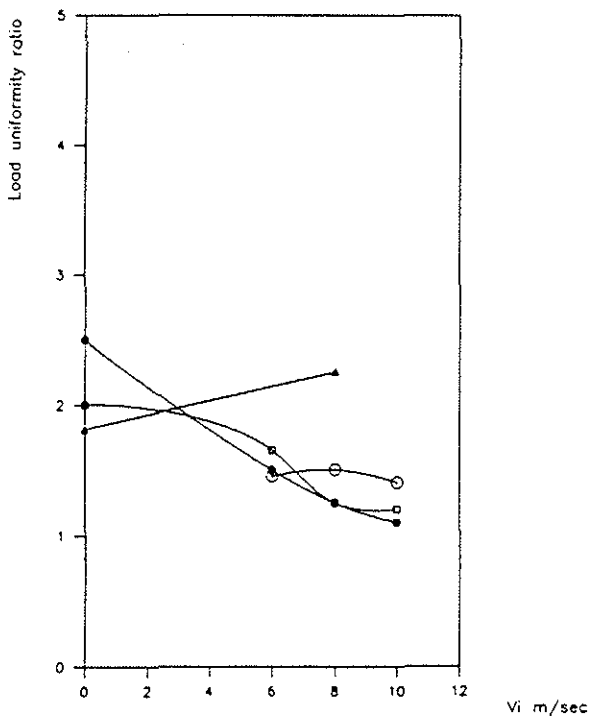


Fig 3: LUR dependence with Vi (graphite unidirectional)

Fig 4: SEA dependence with D/t (graphite fabric)

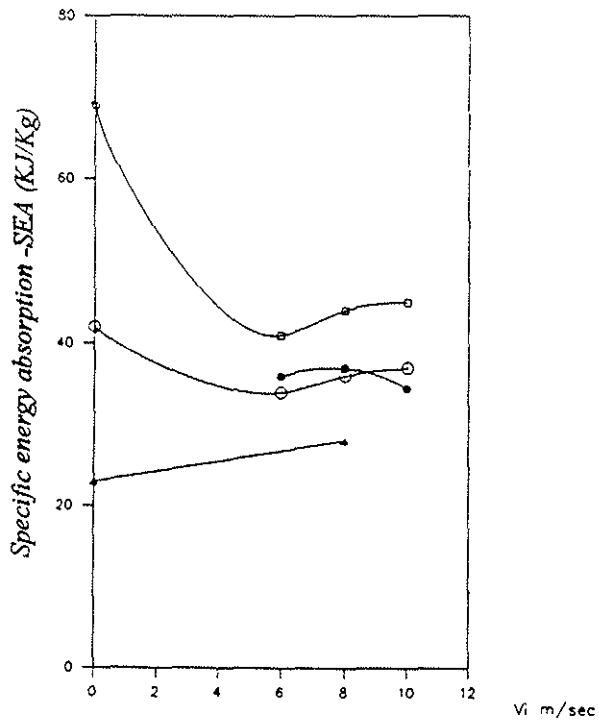


Fig 5: SEA dependence with V_i (graphite fabric)

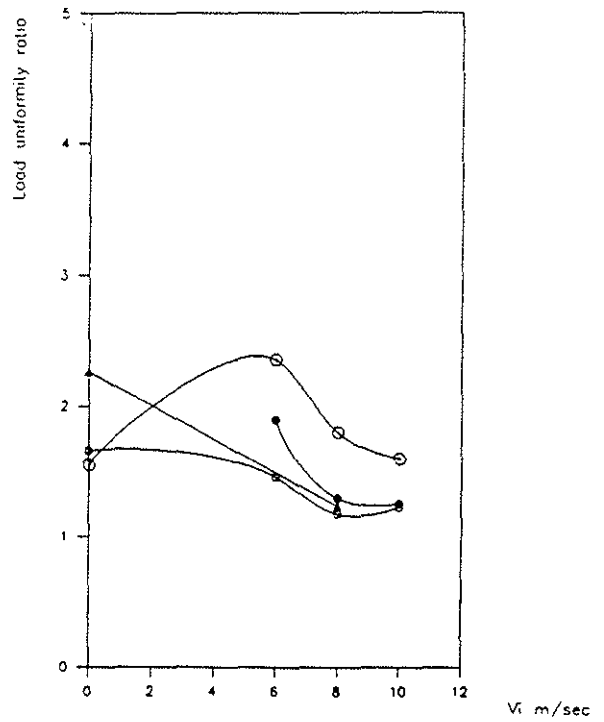


Fig 6: LUR dependence with V_i (graphite fabric)

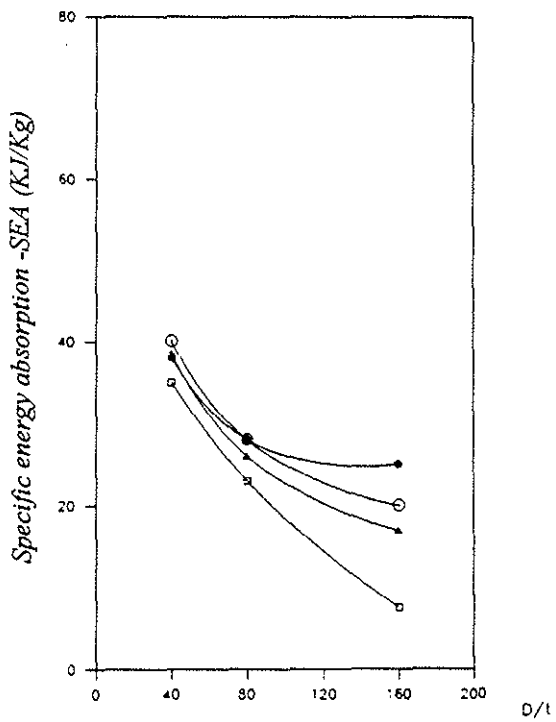


Fig 7: SEA dependence with D/t (kevlar fabric)

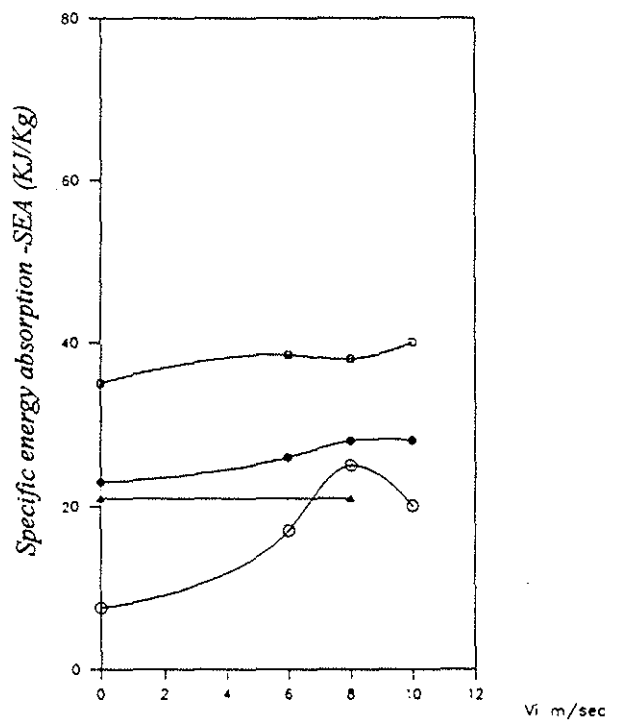


Fig 8: SEA dependence with V_i (kevlar fabric)

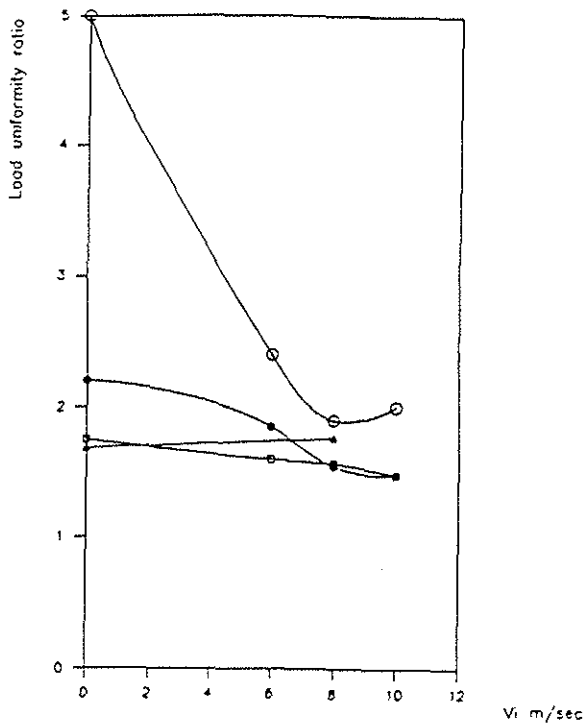


Fig 9 : LUR dependence with Vi (kevlar fabric)

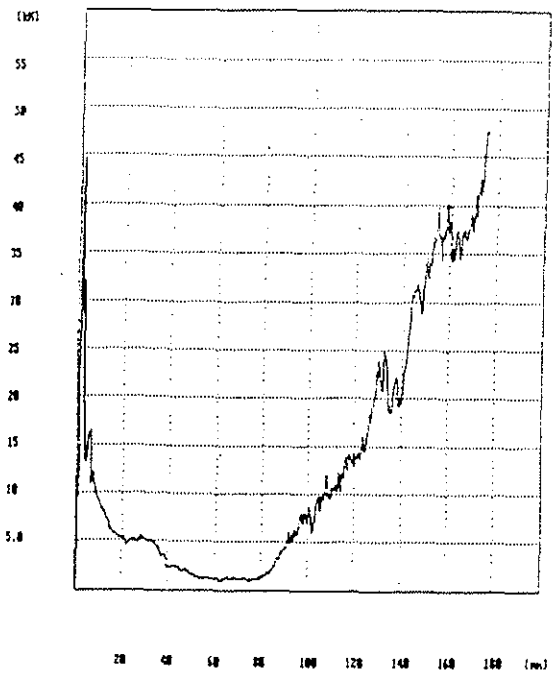


Fig 10: Type A load-displacement static curve

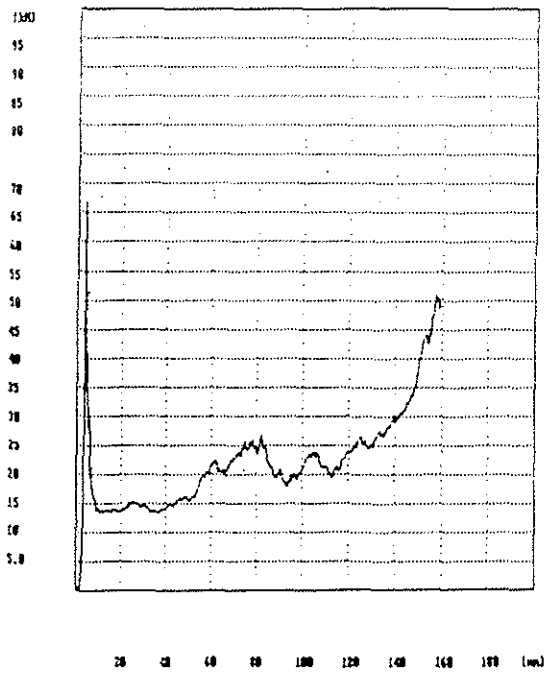


Fig 11 Type B load-displacement static curve

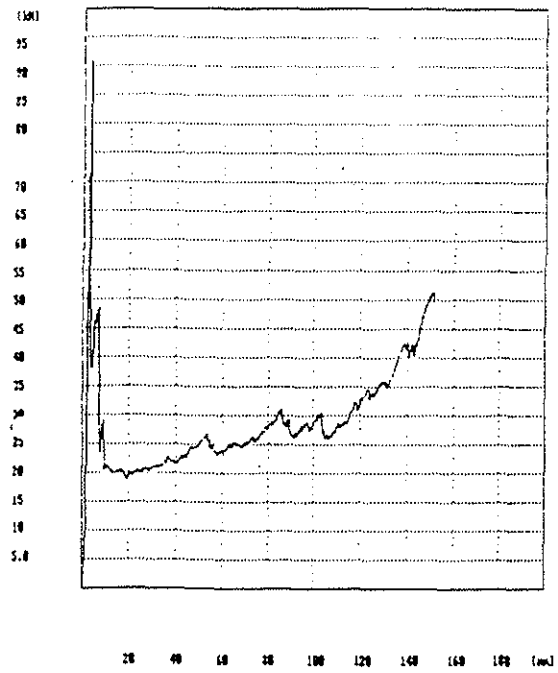


Fig 12 Type C load-displacement static curve

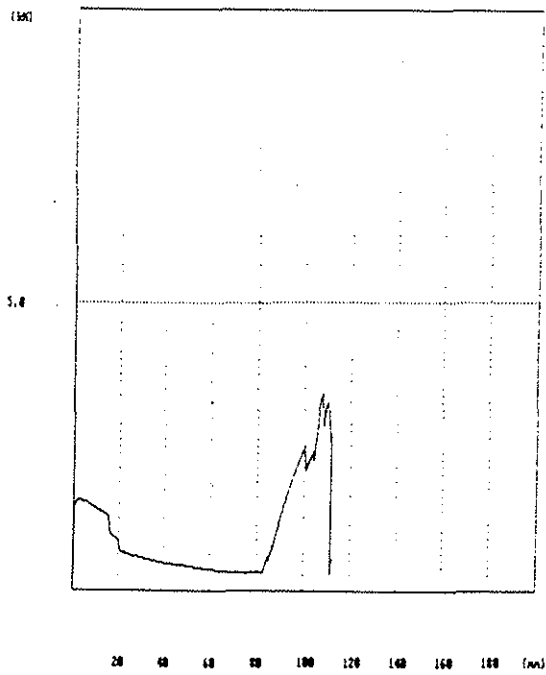


Fig 13 Type A load-displacement static curve

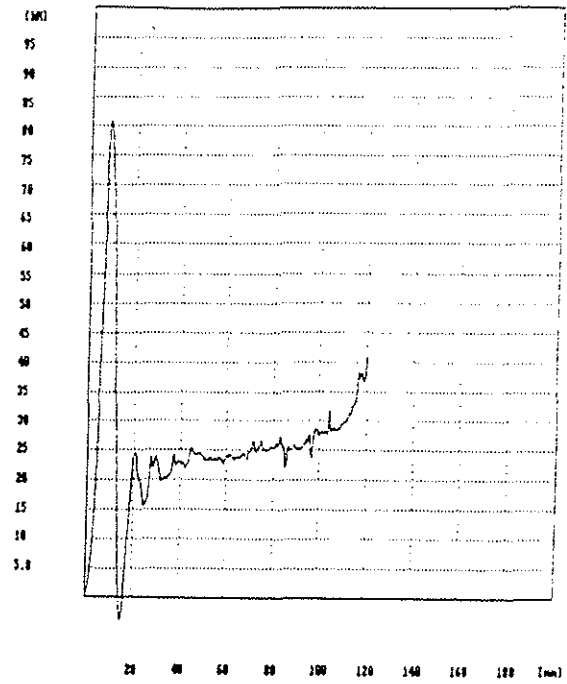


Fig 14: Type A load-displacement dynamic curve

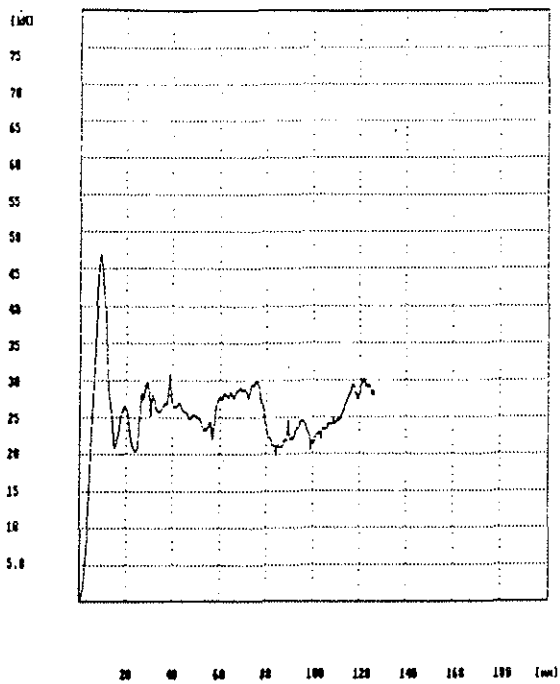


Fig 15: Type B load-displacement dynamic curve

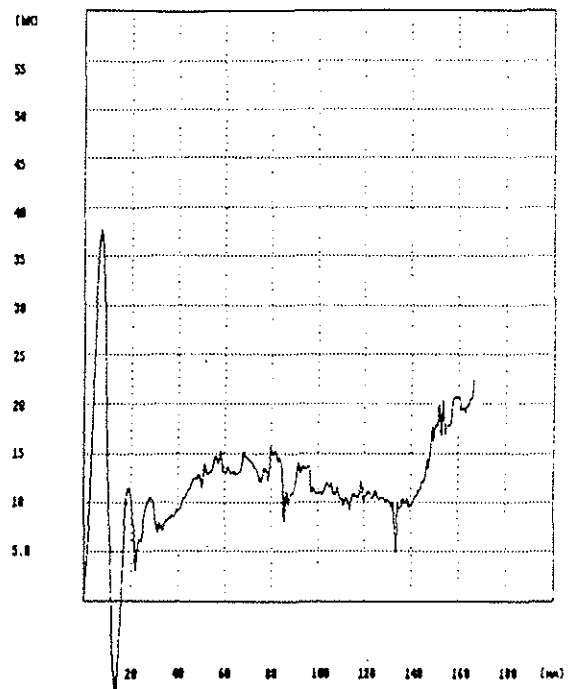


Fig 16: Type C load-displacement dynamic curve

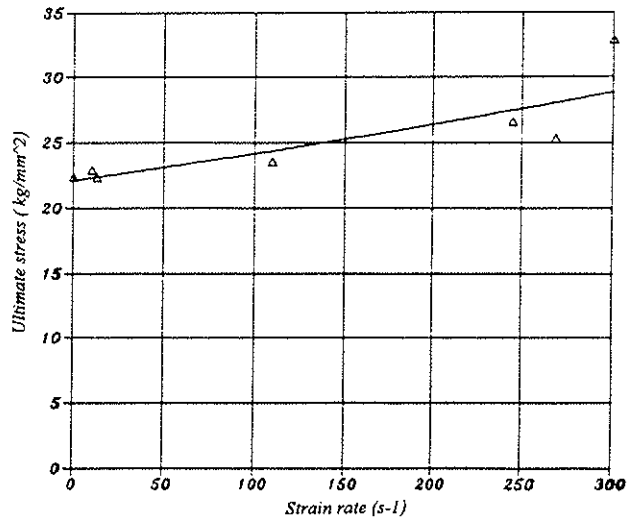
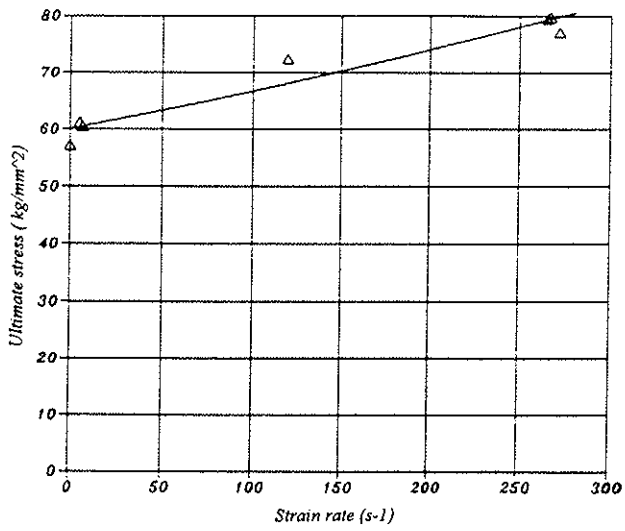


Fig 17 : Ultimate stress-strain rate, graphite fabric [0°]

Fig 18 : Ultimate stress-strain rate, graphite fabric [45°]

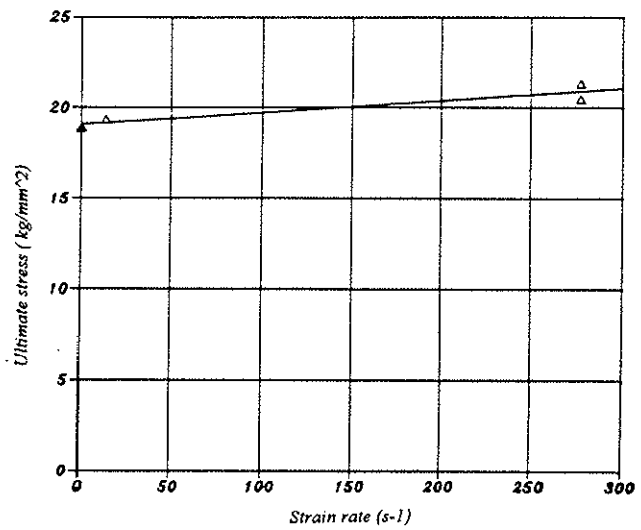
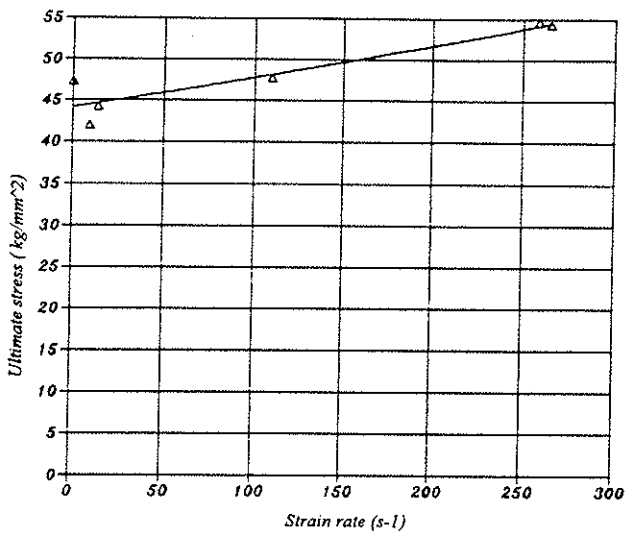


Fig 19 : Ultimate stress-strain rate, kevlar fabric [0°]

Fig 20 : Ultimate stress-strain rate, kevlar fabric [45°]

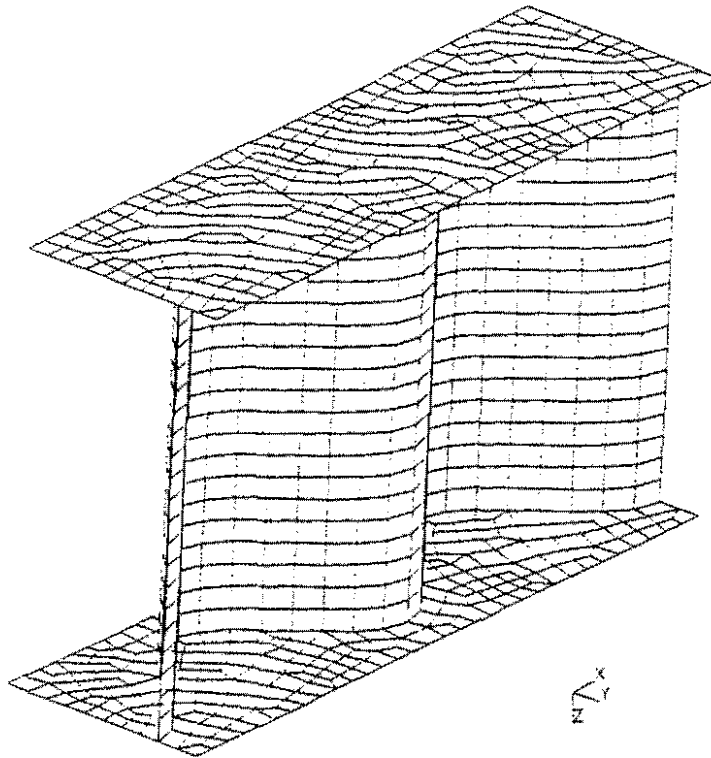
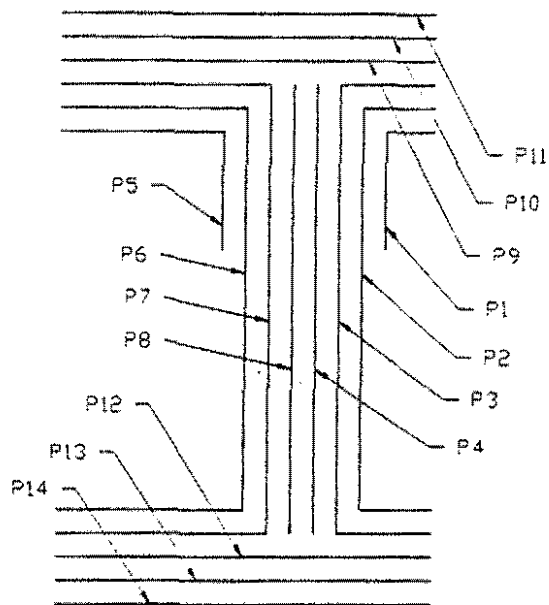


Fig 21 : Sine wave beam finite element model



P1-P2-P5-P6-P11-P14 kevlar fabric [45°]
 P3-P7 graphite fabric [45°]
 P4-P8-P9-P10-P12-P13 graphite tape [0°]

Fig 22 : Sine wave beam lamination

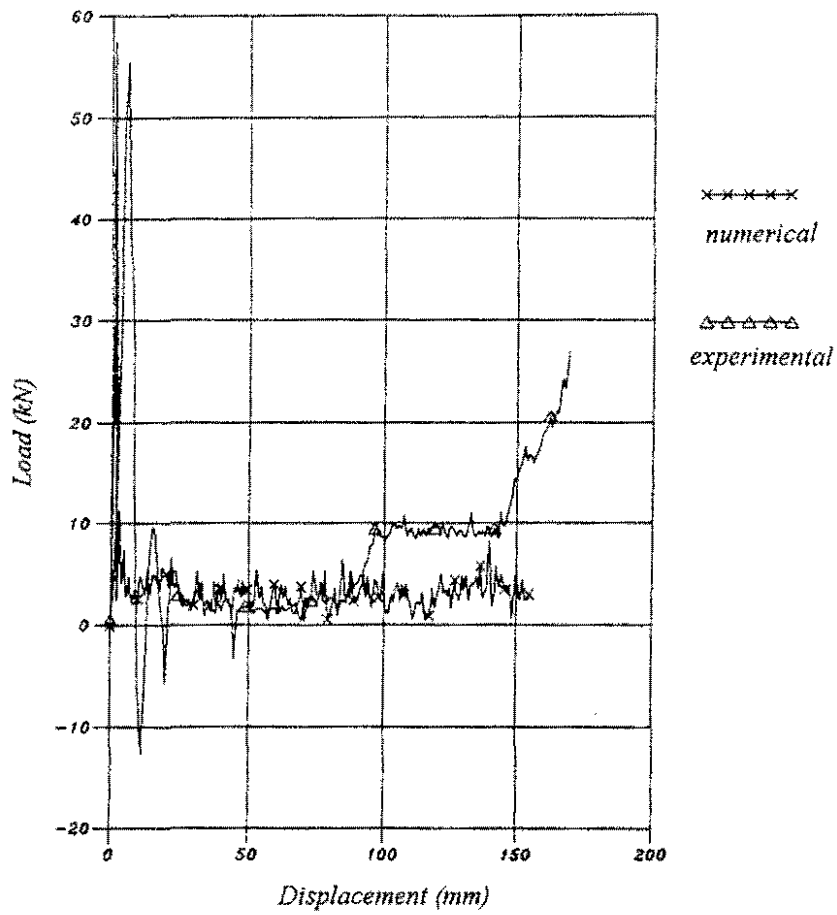


Fig 23 : Sine wave beam experimental and numerical load-displacement curve

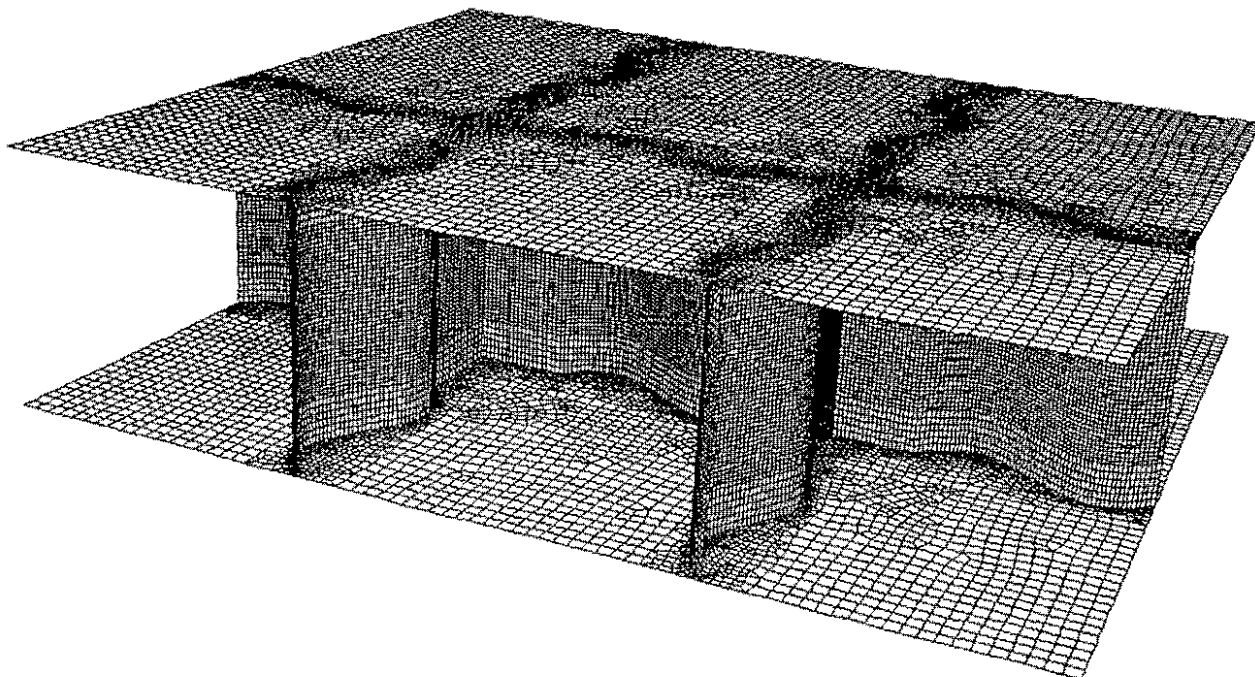


Fig 24 : Complete subfloor finite element model